I R A M P
14(1), Jan 2023, pp. 7-16

ISSN: 2229-39-44

Laser Plasma Cyanide Emission Spectra Analysis

CHRISTIAN G. PARIGGER

Physics and Astronomy Department, University of Tennessee,
University of Tennessee Space Institute, Center for Laser Applications,
411 B.H. Goethert Parkway, Tullahoma,
TN 37388-9700, USA; cparigge@tennessee.edu

ABSTRACT: This work communicates analysis of cyanide, CN, laser-plasma emission records using line strength data, the ExoMol astrophysical database, standard molecular parameters, a laser-induced fluorescence database, in conjunction with a nonlinear fitting code and a program for simulating diatomic molecular spectra. Predicted cyanide spectra of the $\mathrm{CN,\ B\ ^2\Sigma^+ \longrightarrow X\ ^2\Sigma^+,\ \Delta v = 0}$ sequence compare nicely with 33 picometer resolution experimental results. The analysis focuses on experiment data captured with 1064-nm, 35-ps pulse-width bursts within an overall 1 nanosecond pulse envelope. The accuracy of the CN line strength data is better than one picometer. This work compares experiment results with predictions for equilibrium of rotational and vibrational modes and at an internal, molecular temperature of the order of 8,000 Kelvin. Accurate CN synthetic spectra and applications in combustion diagnosis, chemistry, supersonic and hypersonic expansion diagnosis, and in the study of astrophysical phenomena.

Kewords: diatomic molecules; cyanide; laser-plasma; data analysis; laser induced breakdown spectroscopy; combustion; time-resolved spectroscopy; spectra fitting program; astrophysics

1. INTRODUCTION

The diatomic molecule cyanide, CN, occurs in various forms in nature. Toxicity of cyanide motivates health studies, in particular those of hydrogen cyanide gas that can be lethal by inhalation. Cyanide radical measurements characterize interstellar clouds including temperature inferences of the cosmic microwave background radiation [1, 2]. The primary interest in this work is the CN violet $B\,^2\Sigma^+ - X\,^2\Sigma^+$ band system. Extensive experimental and theoretical details convey the complexity of the CN radical [3, 4]. The CN red systems are mentioned in a study of laboratory spectroscopy of astrophysically interesting molecules [5].

Spectroscopy [6-10] of laser-induced air plasma reveals fingerprints" of CN early (within the first microsecond) in the plasma decay [11]. This work investigates existing databases for diatomic molecules, in particular the ones for CN, for analysis of measured emission spectra. Laser-induced breakdown with 6-ns, 1064-nm radiation and associated diagnosis [12] discusses determination of CN distribution and shock-wave phenomena in hypersonic and supersonic expansion.

For cyanide spectroscopy, one can employ the ExoMol database [13], the LIFBASE laser induced fluorescence database [14], and the PGOPHER program for simulating rotational, vibrational and electronic spectra [15]. There are of course other databases that can be accessed [16] for diatomic molecules, including HITEMP that for example shows hydroxyl, OH, data [17]. The ExoMol, LIFBASE, PGOPHER predictions of the CN violet v = 0 sequence are compared with experimental data. The laser-plasma recombination spectra that are utilized in the comparisons were captured following optical breakdown with picosecond laser pulses in a 1:1 molar CO_2:N_2 atmospheric gas mixture and in standard ambient temperature and pressure laboratory conditions. Astrophysical ExoMol databases are expected to work well for optical spectroscopy of laser-plasma. The measurement of molecular spectra may be accomplished

with nanosecond laser-induced optical breakdown - molecular spectra are readily observed with femtosecond or picosecond laser-plasma excitation - after some time delay (of the order of larger than 100 ns for occurrence of CN in CO_2:N_2 gas mixtures) from optical breakdown when using nanosecond laser pulses. In addition, analysis is discussed with previously established line-strength data that are freely available along with MATLAB [18] scripts for a subset of transitions associated with the CN violet and red band systems [19, 20].

2. EXPERIMENTAL AND ANALYSIS DETAILS

Computation of optical molecular spectra relies on sets of wavelength positions and line strengths for molecular band systems with in principle theoretically resolved vibrational and rotational transitions. This work focuses on data captured with an experimental spectral resolution of 0.033 nm. Consequently, there are a multitude of lines for each wavelength-bin of a digital array detector that captures time-resolved data following individual laser-plasma events. For example, there are well over 2,000 lines in the CN violet Δv = 0 spectral region of 370 nm to 390 nm, and most lines are bunched together including overlapped vibrational band heads. The measurements utilize a typical laser-induced optical breakdown experimental arrangement [21], namely, (i) laser device, (ii) focusing lens, (iii) cell that contains the atmospheric mixture, (iv) spectrometer, (v) linear diode detector and optical multichannel analyzer, (vi) electronic timing, and (vii) monitor devices and equipment for subsidiary measurements capturing time-resolved CN B-X data.

A. Traditional simulation of diatomic molecular spectra

The traditional approach for the generation of simulated spectra is based on molecular constants. The energy levels can be evaluated by employing a Dunham expansion [22],

$$E(\mathrm{v}, J) = \sum_{k,l} Y_{k,l}(\mathrm{v}+1/2)^k[J(J+1)]^l. \tag{1}$$

The constant coecients $Y_{k,l}$ are called Dunham parameters, with the indices k and l corresponding to vibrational and rotational contributions, respectively. The k = 0 and l = 0 parameter $Y_{0,0}$ represents the minimum electronic energy, T_e. Table I lists the molecular constants in units of cm^{-1} for the A-X and B-X transitions for $^{12}C^{14}N$ [23].

The application of traditional molecular constants (see Table I) is expected to reveal line-position and intensity inconsistencies. For example, air emission spectra predictions with the non-equilibrium air radiation (NEQAIR) code [24, 25] reveal slightly different line positions leading to difficulties in air-plasma analysis of superposition spectra composed of several species. The laser plasma that is generated in dry air shows a variety of species [26-28], consequently, accurate predictions of individual components are desirable. Recently, commercial SPECAIR software is available that focuses on calculating emission or absorption

Table 1. Spectroscopic constants for the A-X and B-X transitions of $^{12}C^{14}N$.

$Y_{k,l}$	Constant	$X^2\Sigma^+$ (cm^{-1})	$A^2\Pi$ (cm^{-1})	$B^2\Sigma^+$ (cm^{-1})
$Y_{0,0}$	T_e	0.	9,245.28	25,752.0
$Y_{1,0}$	ω_e	2,068.59	1,812.5	2,163.9
$-Y_{2,0}$	$\omega_e x_e$	13.087	12.60	20.2
$Y_{3,0}$	$\omega_e y_e$	-0.00909	-0.0118	–
$Y_{0,1}$	B_e	1.8997	1.7151	1.973
$-Y_{1,1}$	α_e	0.01736	0.01708	0.023
$Y_{2,1}$	γ_e	-3.10×10^{-5}	-3.6×10^{-5}	–
$-Y_{0,2}$	D_e	6.40×10^{-6}	5.93×10^{-6}	$[6.6 \times 10^{-6}]$
$-Y_{1,2}$	β_e	1.2×10^{-9}	42×10^{-9}	–

spectra of air plasma radiation [29]. Conversely, one can utilize published molecular line positions and strengths for individual species for the spectra simulation of the CN diatomic molecule.

B. Line positions and strengths of diatomic spectra

In this work, the computation of diatomic molecular spectra utilizes line strength data. The Boltzmann equilibrium spectral program (BESP) and the Nelder-Mead temperature (NMT) program allow one to respectively compute an emission spectrum and fit theoretical to experimental spectra. The construction of the communicated molecular CN line strengths "CNv-lsf" [20] first, makes use of Wigner-Witmer eigenfunctions and a diatomic line position fitting program, second, computes Frank-Condon factors and r-centroids, and third, combines these factors with the rotational factors that usually decouple from the overall molecular line-strength due to the symmetry of diatomic molecules. In turn, the ExoMol states and transition files for CN [4, 30, 31] and the PGOPHER data file [32] are examined in order to generate line strength data that can be used with BESP and NMT. The LIFBASE program is utilized for visual comparisons of CN B-X simulated and recorded data.

The ExoMol and the PGOPHER data show Einstein A-coecients that are converted to line strengths [33-35], S, for electric dipole transitions, using

$$A_{ul} = \frac{16\pi^3}{3g_u h\epsilon_0 \lambda^3} (e\ a_0)^2\, S_{ul}, \qquad g_u = 2(2J_u + 1). \tag{2}$$

Here, A_{ul} denotes the Einstein A-coefficient for a transition from an upper, *u*, to a lower, *l*, state, and *h* and ε_0 are Planck's constant and vacuum permittivity, respectively. The elementary charge is *e*, the Bohr radius is a_0, and the transition strength is S_{ul}. The line strength, *S*, that is used in the MATLAB scripts is expressed in traditional spectroscopy units (stC^2 cm^2). The wavelength of the transition is λ, g_u is the upper state degeneracy and J_u the total angular momentum of the upper state. In the establishment of line strength data, Hund's case (a) basis functions are preferred in connection with application of the Wigner and Witmer [36, 37] diatomic eigenfunction.

The prediction of diatomic spectra and establishment of the CNv-lsf database involves (a) determination of accurate wavenumbers for the transition and rotational line strengths, viz. Hönl-London values, (b) vibrational transition strengths, viz. Frank-Condon factors, from eigenfunctions for the diatomic potential, (c) expansion of the electronic transition moments employing r-centroids. The product of these three factors yields the line strength, or alternatively, the Einstein A-coefficient using Eq. (2).

C. Measured air wavelength vs. vacuum wavenumbers

The PGOPHER program allows versatile fitting of experimental data records by introducing a so-called overlay data set as function of wavenumbers. Experimental data are converted to vacuum wavenumbers using the variation of the refractive index, *n*, of air with wavelength [38],

$$10^6(n-1) = a_0 + \frac{a_1}{\lambda_N^2} + \frac{a_2}{\lambda_N^4}, \tag{3}$$

where N is the wavelength in normal air at 15 °C and 101,325Pa (760mmHg), expressed in terms of micrometer (range 0.2218-0.9000 μm). Table II lists constants for Eq. (3).

For NMT computations however recorded, digital intensity values versus calibrated wavelength are utilized. The variation of the refractive index, r_i, of air at 15 °C, 101,325 Pa, and 0% humidity, with wavenumber [39],

TABLE 2. Constants for variation of refractive index, *n*, see Equation 3.

Parameter	Value
a_0	272.643
a_1	1.2288 (μm^2)
a_2	0.03555 (μm^4)

$$10^8(r_i - 1) = \frac{k_1}{(k_0 - \sigma^2)} + \frac{k_3}{(k_2 - \sigma^2)}, \tag{4}$$

where σ is the wavenumber in units of μm^{-1}, allows one to compute air wavelengths from the vacuum wavenumbers. Table III lists constants in Eq. (4).

TABLE 3. Constants for variation of refractive index, see Equation 4.

Parameter	Value (μm^{-2})
k_0	238.0185
k_1	5,792,105
k_2	57.362
k_3	167,917

3. RESULTS

This section elaborates analysis of recorded CN spectra of the $B\,^2\Sigma^+ \longrightarrow X\,^2\Sigma^+, \Delta v = 0$ sequence. The spectra were captured using an intensified 1024-diode array detector and a laboratory-type Czerny-Turner (Jobin Yvon model HR-640) spectrometer. The spectral resolutions of the experimental arrangement amounts to 0.033nm ($\simeq 2\ cm^{-1}$)for the employed 3600 groves/mm grating. Detector sensitivity corrections and wavelength calibrations were accomplished with standard spectroscopic light sources. The time-resolved measurement gate-delays were 400 nanosecond (ns), with gate-open times of 500 ns. An average of 40 spectra were collected, consequently, the inferred temperature is an average of the line-of-sight data during the gate-open duration.

The analysis discusses the fitting results obtained with (A) the PGOPHER program using PGOPHER data, (B) the NMT program using PGOPHER- and ExoMol- line strengths, (C) the NMT program using CNv-lsf data, and (D) the LIFBASE program.

One of the primary interests is the use of updated ExoMol sets of line strength data that appear to be in use for extragalactic studies [31]. Availability of an extensive line list obviously would alleviate computation of specific transitions that are investigated in laserplasma laboratory experiments, including CN B-X violet and CN A-X red systems. The ExoMol database shows 2,285,103 transitions up to 60,000 cm^{-1} between the three lowest electronic states, $X\ ^2\Sigma^+, A\ ^2\Pi,$ and $B\ ^2\Sigma^+$. The PGOPHER dataset for CN A-X and B-X includes 191,109 transitions.

The CNv-lsf and CNr-lsf data contain 7,960 and 40,728 transitions, respectively. The differences in number of transitions are in part due to the number of rotational states (up to $\simeq$ 120 in ExoMol), the values for Einstein A-coefficients and associated line strengths (see Eq. (2)), or the establishment of sets of computed molecular parameters that fit data from high-resolution, Fourier-transform spectroscopy. The line positions are determined from high-resolution data with a standard deviation comparable to the estimated experimental errors. The obtained, simulated line strengths are typically better than 0.05 cm^{-1}.

A. PGOPHER program using PGOPHER data

The full CN B-X and A-X transition data are available for the construction of simulated spectra. Figure 1 displays measured and fitted CN violet spectra. The fitted spectrum also shows the baseline correction and difference between experimental and simulated spectra.

The synthetic spectrum is fitted using the PGOPHER program and an overlay of the experimental record of recorded optical multichannel analyzer (OMA) counts versus vacuum wavenumbers that are computed from the

recorded air wavelengths. Table IV lists results for parameters that were selected for fitting. Normalized intensity units were used, i.e., the partition function is implemented. Following a separate fit for determination of the wavenumber offset of -0.31 cm^{-1} (-0.005 nm - the Doppler width at $\simeq$ 8,000 K for CN equals $\simeq$ 0.005 nm), the selected parameters included Gaussian width, temperature, scaling, and T_{vib} that assesses deviation from thermodynamic equilibrium. The T_{vib} results confirms Boltzmann distribution equilibrium within the standard deviation.

In this work, a Gaussian profile models the spectrometer and intensified linear-array detector transfer function. However, a measured system transfer function or a Voigt function

TABLE 4. PGOPHER tting parameters and results.

Parameter	Value	Standard Deviation
Temperature (K)	8,103	187
Gaussian width (cm^{-1})	2.2	0.03
Scale (a.u.)	43,960	790
T_{vib} (K)	8,108	146

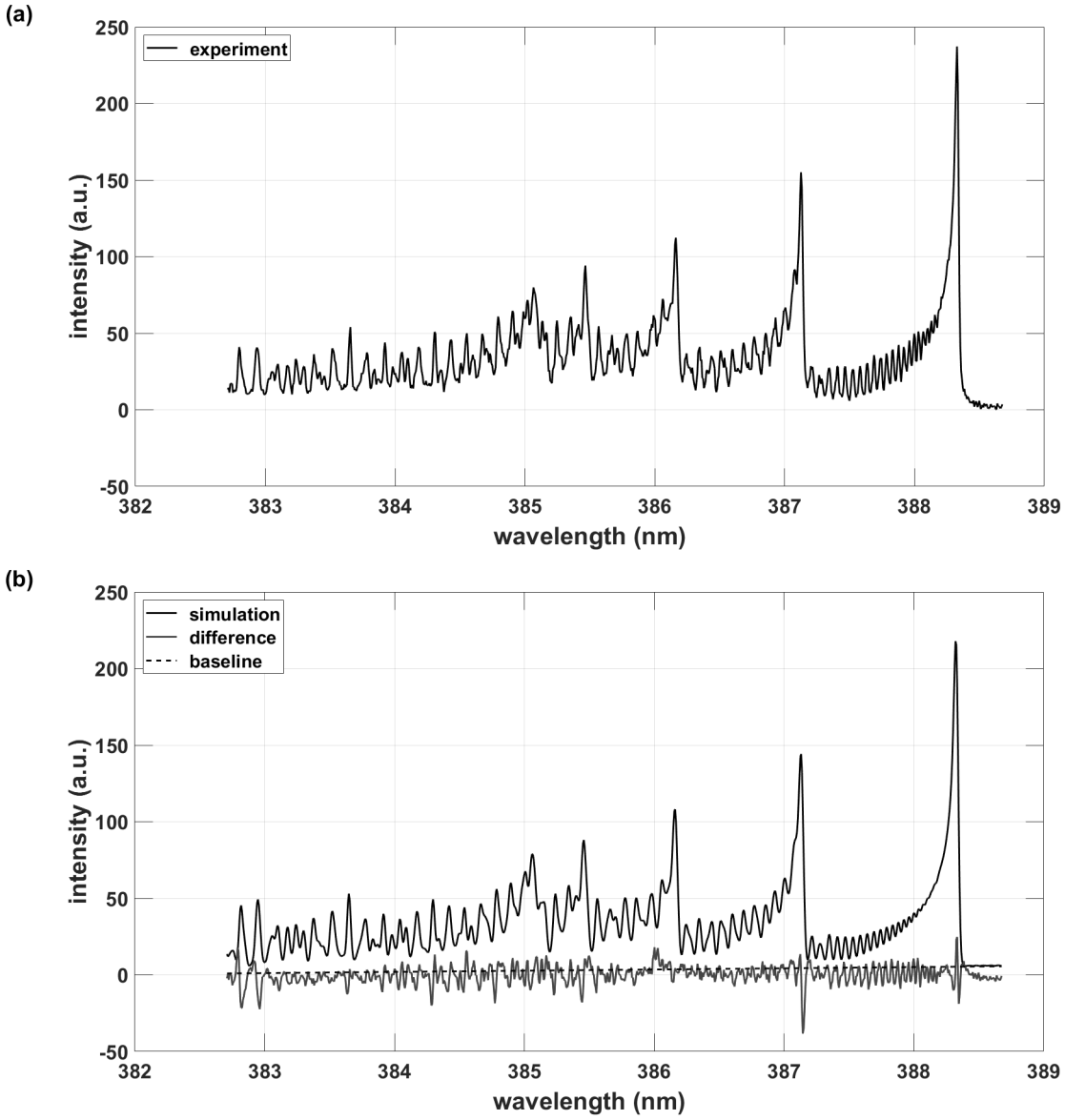

FIG. 1. (a) Experimental spectrum. (b) Simulation with PGOPHER, T = 8103 K, $\triangle\lambda$ = 0.033 nm.

can replace the selected Gaussian profile provided that changes are implemented in the MATLAB source scripts for the recently communicated BESP and NMT scripts [20]. The PGOPHER program allows one to accomplish Voigt profile fits.

Investigations of tting Gaussian, w_G, and Lorentzian, w_L, widths, while leaving all other parameters constant, leads to the PGOPHER results w_G = 1.6 cm^{-1} (0.024 nm) and w_L = 0:64 cm^{-1} (0.0095 nm). Application of an empirical Voigt width, w_V, approximation [40],

$$w_V \approx w_L/2 + \sqrt{w_L^2/4 + w_G^2}, \tag{5}$$

results in $w_V \approx$ 2.0 cm^{-1} (0.029 nm). The widths in units of nm that are indicated in brackets are calculated using $\Delta\lambda = \Delta\tilde{\nu} \times \lambda^2$ at a wavelength of 386 nm (central wavelength of the data). The Lorentzian contribution to the Voigt profile amounts to $\approx$ 30 per cent.

B. NMT program using PGOPHER- and ExoMol- line strengths

In addition, CN B-X line positions and Einstein A-coecients (that are converted to line strengths) are collected in a data file that is compatible with the mentioned NMT-spectral fitting program.

Figure 2 illustrates spectra determined from temperature and Gaussian linewidth fitting. The results are consistent with those obtained from the versatile PGOPHER program. The inclusion of CN A-X data in the analysis would change the inferred temperature by $\simeq$ 0.1%.

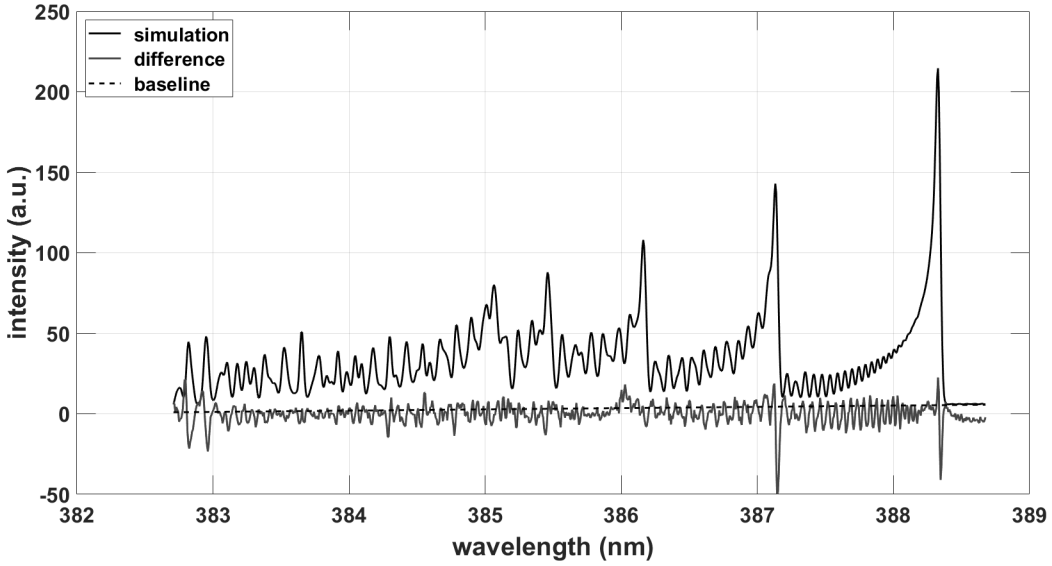

FIG. 2. Simulation using PGOPHER data and the NMT program, T = 8240 K, $\Delta\lambda$ = 0.034 nm.

Similarly, the recommended ExoMol databases for states and transitions were utilized to generate a subset of lines and strength for analysis with the NMT program. The results displayed in Fig. 3 indicate a Gaussian full-width-at-half-maximum (FWHM) of 0.038 nm, indicative of line-position differences in the ExoMol data. However, the inferred temperature appears consistent with the results illustrated in Figs. 1 and 2.

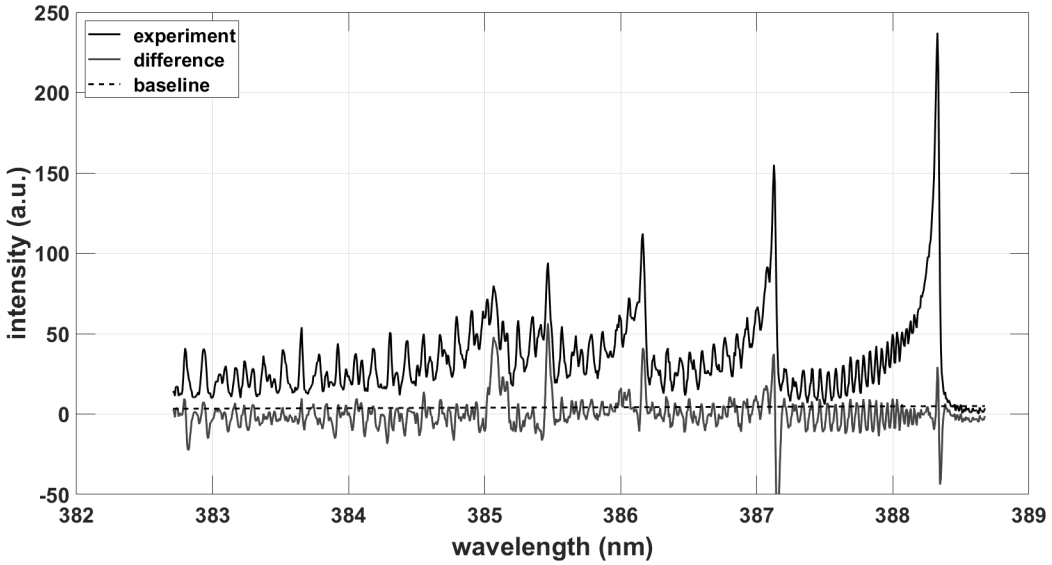

FIG. 3. Simulation using ExoMol data and the NMT program, T = 8150 K, $\Delta\lambda$ = 0:038 nm.

C. NMT program using CNv-lsf data, comparisons

Analysis of the measured data with the CNv-lsf data reveals a temperature of T = 8140 K, and a tted FWHM of 0.038 nm. Figure 4 shows the fitting results.

The simulated spectra in Figs. 1, 2, 3, and 4, display superposition spectra from quite a few individual rotational-vibrational transitions of the CN B-X $\Delta v = 0$ sequence. Actually, small contributions from the CN A-X transition are also included in the PGOPHER and ExoMol databases. Tables V and VI summarize the number of lines in the data files.

TABLE 5. Number of transitions of the simulated spectra in the measured experimental range (25,725 cm^{-1} to 26,125 cm^{-1}).

Database	CN B-X	CN B-X and A-X
PGOPHER	3,598	5,631
ExoMol	4,302	17,181
CNv-lsf	2,461	2,461

TABLE 6. Number of transitions of the simulated spectra in the measured experimental range (see Tab. V) with Einstein A-coefficients larger than 10^3 s^{-1}.

Database	CN B-X	CN B-X and A-X
PGOPHER	3,205	4,532
ExoMol	3,625	8,270
CNv-lsf	2,461	2,461

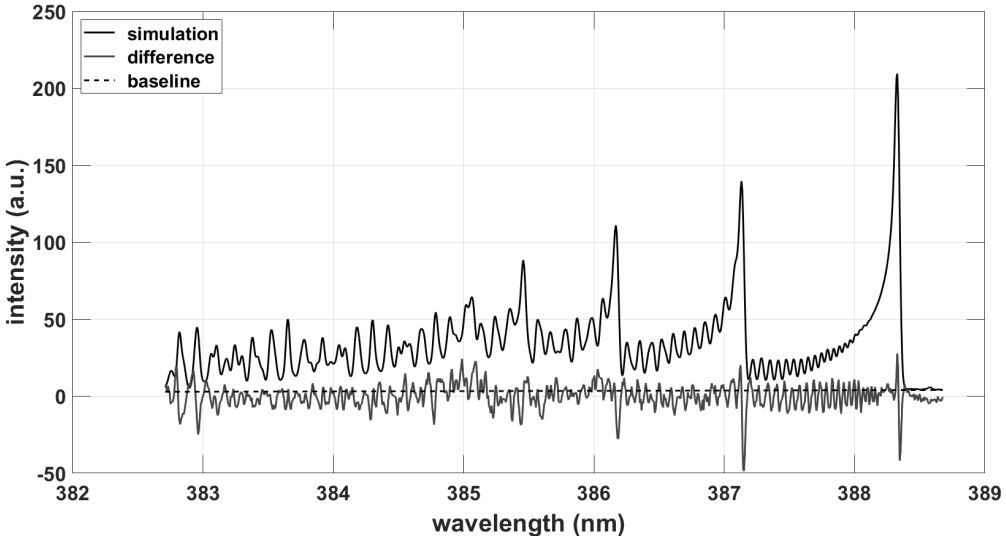

FIG. 4. Simulation using CNv-lsf data and the NMT program, T = 8140 K, $\triangle\lambda$ = 0.036 nm.

Comparisons of CN B-X line position accuracies in the PGOPHER and ExoMol databases with those of the CNv-lsf database are further elaborated for the experiments (25,725 cm^{-1} to 26,125 cm^{-1}) and for Einstein A-coefficients larger than 10^3 s^{-1} (see first column in Tab. VI). Table VII displays agreements of lines within the indicated wavenumber range and otherwise the same angular momentum values for upper and lower levels of the transitions.

TABLE 7. Subset CN B-X lines of the PGOPHER and ExoMol data that agree within $\Delta\tilde{\nu}$ of 2,461 CN B-X transitions in the CNv-lsf data for the experiment (25,725 cm^{-1} to 26,125 cm^{-1}).

Database	$\Delta\tilde{\nu} < 0.05\text{cm}^{-1}$	$\Delta\tilde{\nu} < 0.2\text{cm}^{-1}$	$\Delta\tilde{\nu} < 1.0\text{cm}^{-1}$	$\Delta\tilde{\nu} < 2.0\text{cm}^{-1}$
PGOPHER	1,200	1,422	1,823	2,012
ExoMol	158	463	1,266	1,935

Various aspects of the accuracy of the CNv-lsf database have been extensively tested [19] including analysis of laser-induced fluorescence and nominal 300 K temperature Fourier transform spectra. The differences in predictions for line positions appears larger for levels with higher angular momenta, *J'* and *J*. The accuracy of line positions in the CNv-lsf database is better than 0.05 cm^{-1}. Table VII reveals that PGOPHER line positions compare favorably with those in the CNv-lsf database. The ExoMol database appears acceptable within $\simeq$ 2 wavenumbers that corresponds to a spectral resolution of $\simeq$ 0.033 nm. However, high-temperature ($\simeq$ 8,000 K) inferences from CN B-X spectra at a 0.033-nm experimental spectral resolution appear only minimally affected (see Figs. 2 and 3).

D. LIFBASE program

The LIFBASE program is also used for simulation of the measured spectrum. A Voigt profile of width 0.033 nm with a 30% Lorentzian contribution is selected. Figure 5 illustrates the results. Noteworthy is that the PGOPHER program is capable of fitting Voigt proles as well. However, Gaussian proles are usually selected in the NMT program for modeling of the spectrometer & detector transfer function. The choice of a 30% Lorentzian contribution is based on PGOPHER-program investigations, see Eq. (5).

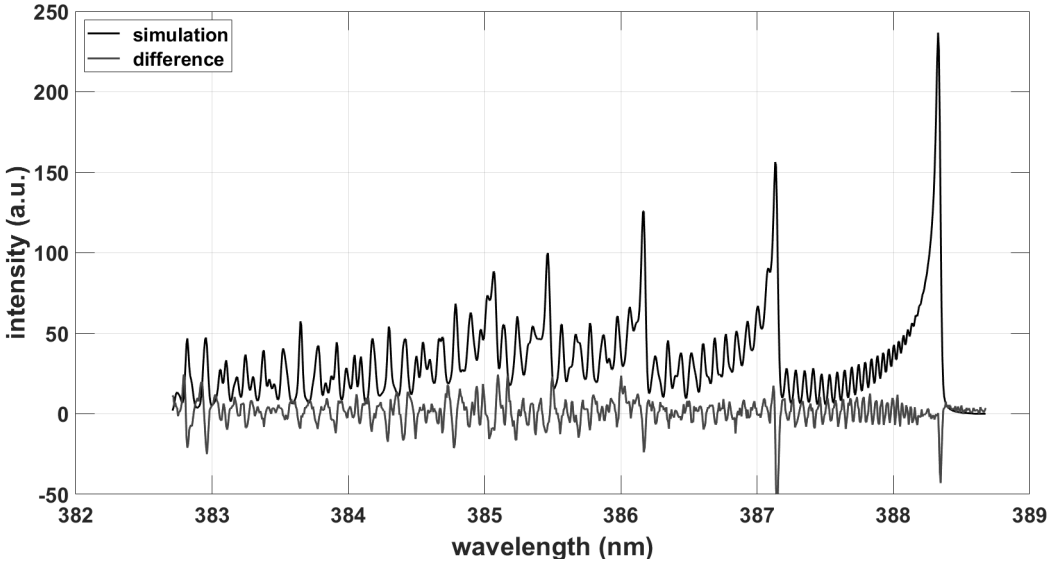

FIG. 5. Simulation using LIFBASE with xed T = 8103 K, $\triangle\lambda$ = 0:033 nm, Voigt prole with 30% Lorentzian contribution.

4. DISCUSSION

The CN violet $B\,^2\Sigma^+ - X\,^2\Sigma^+,\ \Delta \mathrm{v} = 0$ sequence reveals a multitude of vibrational and rotational transitions that are usually not individually resolved in the study of laser-induced plasma emissions in the spectral range of 383 nm to 389 nm. Analysis of the 0.033-nm spectral resolution experimental emission spectrum with the PGOPHER program and use of full CN B-X data file yields CN excitation temperature of $\simeq$ 8,100 K and a standard deviation of $\simeq$ 200 K.

Similar results are obtained when using the CN B-X data in conjunction with a Nelder- Mead spectral fitting program. The most recent ExoMol CN data also predict a temperature within the standard deviation of the PGOPHER prediction, but there appear to be discrepancies in the ExoMol predictions near the 2-2, 3-3, and 4-4 band heads, or in the range of 385 nm to 386 nm. Analogous results are noted when using the CNv-lsf line strengths with however slightly better agreement of experimental and simulated spectra than those for ExoMol. Comparative spectra obtained from the LIFBASE program are as well largely in agreement with the measured data. The expansive PGOPHER and ExoMol line lists allow one to predict simulated spectra consistent with laboratory laser-plasma experiments.

ACKNOWLEDGMENTS

The author (CGP) acknowledges the support in part by the Center for Laser Applications at the University of Tennessee Space Institute.

References

[1] Roth, K.C.; Meyer, D.M.; Hawkins, I. Astrophys. J. 413, L67, (1993).

[2] Leach, S. Can. J. Chem 82, 730, (2004).

[3] Ram, R.S.; Davis, S.P.; Wallace, L.; Englman R.; Appadoo, D.R.T.; Bernath, P.F. J. Mol. Spectrosc. 37, 225, (2006). Applications; IOP Publishing: Bristol, UK, 2020.

[4] Brooke, J.S.A.; Ram, R.S.; Western, C.M.; Li, G.; Schwenke, D.W.; Bernath, P.F. Astrophys. J., Suppl. Ser. 210, 1, (2014).

[5] Davis, S.P. Publ. Astron. Soc. Pac. 1987, 99, 1105.

[6] Kunze, H.-J. Introduction to Plasma Spectroscopy; Springer: Berlin/Heidelberg, Germany, 2009.

[7] Fujimoto, T. Plasma Spectroscopy; Clarendon Press; Oxford, UK, 2004.

[8] Ochkin, V.N. Spectroscopy of Low Temperature Plasma; Wiley-VCH: Weinheim, Germany, 2009.

[9] Demtröder, W. Laser Spectroscopy 1: Basic Principles, 5th ed.; Springer: Heidelberg, Germany, 2014.

[10] Demtröder, W. Laser Spectroscopy 2: Experimental Techniques, 5th ed.; Springer: Heidelberg, Germany, 2015.

[11] Miziolek, A.W., Palleschi, V., Schechter, I. (Eds.) Laser Induced Breakdown Spectroscopy (LIBS): Fundamentals and Applications; Cambridge Univ. Press: New York, NY, USA, 2006.

[12] Singh, J.P.; Thakur, S.N. (Eds.) Laser-Induced Breakdown Spectroscopy, 2nd ed.; Elsevier: Amsterdam, The Netherlands, 2020.

[13] Tennyson, J.; Yurchenko, S.N.; Al-Refaie, A.F.; Clark, V.H.J.; Chubb, K.L.; Conway, E.K.; Dewan, A.; Gorman, M.N.; Hill, C.; Lynas-Gray, A.E.; Mellor, T.; McKemmish, L.K.; Owens, A.; Polyansky, O.L.; Semenov, M.; Somogyi, W.; Tinetti, G.; Upadhyay, A.; Waldmann, I.; Wang, Y.; Wright, S.; Yurchenko, O.P. J. Quant. Spectrosc. Radiat. Transf. 255, 107228, (2020).

[14] Luque, J.; Crosley, D.R. LIFBASE: Database and Spectral Simulation for Diatomic Molecules. 2021. Available online https://www.sri.com/platform/lifbase-spectroscopy-tool (accessed on 25 November 2019).

[15] Western, C.M. J. Quant. Spectrosc. Radiat. Transf. 186, 221, (2017).

[16] McKemmish, L.K. WIREs Comput. Mol. Sci. 11, e1520, (2021).

[17] Rothman, L.S.; Gordon, I.E.; Barber, R.J.; Dothe, H.; Gamache, R.R.; Goldman, A.; Perevalov, V.I.; Tashkun, S.A.; Tennyson, J. J. Quant. Spectrosc. Radiat. Transf. 2010, 111, 2139.

[18] MATLAB Release R2022a Update 5, The MathWorks, Inc.: Natick, Massachusetts, US, 2022.

[19] Parigger, C.G.; Hornkohl, J.O. Quantum Mechanics of the Diatomic Molecule with Applications; IOP Publishing: Bristol, UK, 2020.

[20] Parigger, C.G. Foundations 3, 1, (2023).

[21] Hornkohl, J.O.; Parigger, C.G.; Lewis, J.W.L. J. Quant. Spectrosc. Radiat. Transf. 46, 405, (1991).

[22] Dunham, J.L. Phys. Rev. 41, 721, (1932).

[23] National Institute of Standards and Technology (NIST) Chemistry WebBook, SRD 69, for the Cyano radical, constants of diatomic molecules. 2021. Available online https://webbook. nist.gov (accessed on 20 February 2023).

[24] Whiting, E.E. Space Administration, Reacting Flow Environments Branch, Ames Research Center, CA, US. Personal communication, 1995.

[25] Whiting, E.E.; Park, C.; Liu, Y.; Arnold, J.; Paterson, J. NEQAIR96, Nonequilibrium and Equilibrium Radiative Transport and Spectra Program: User's Manual. Technical Report NASA RP-1389; NASA Ames Research Center: Moet Field, CA, US, 1996.

[26] Boulous, P.M.I.; Pfender, E. Thermal Plasmas - Fundamentals and Applications; Plenum Press, New York, NY, US, 1994.

[27] McBride, B.; Gordan, S. Interim Revision NASA Report RP-1311, Part I; NASA Lewis Research Center: Cleveland, OH, US, 1994.

[28] McBride, B.; Gordan, S. Interim Revision NASA Report RP-1311, Part II; NASA Lewis Research Center: Cleveland, OH, US, 1996.

[29] Laux, C.O. Radiation and Nonequilibrium Collisional-Radiative Models, von Karman Institute Lecture Series 2002-07, Physico-Chemical Modeling of High Enthalpy and Plasma Flows, Fletcher D.; Charbonnier, J.-M.; Sarma, G.S.R.; Magin, T. (Eds.): Rhode-Saint-Genese, Belgium, 2002.

[30] Syme, A.-M.; McKemmish, L.K. Mon. Notices Royal Astron. Soc. 499, 25, (2020).

[31] Syme, A.M.; McKemmish, L.K. Mon. Notices Royal Astron. Soc. 505, 4383, (2021).

[32] Western, C.M. University of Bristol, Bristol, UK. Personal communication, 2019.

[33] Condon, E.U.; Shortley, G.H. The Theory of Atomic Spectra; Cambridge Univ Press: Cambridge, UK, 1964.

[34] Hilborn, R.C. Am. J. Phys. 50, 982, (1982).

[35] Thorne, A.P. Spectrophysics, 2nd ed.; Chapman and Hall: New York, NY, US, 1988.

[36] Wigner, E.; Witmer, E.E. Z. Phys. 51, 859, (1928).

[37] Wigner, E.; Witmer E.E. On the structure of the spectra of two-atomic molecules according to quantum mechanics. In Hettema H. (Ed) Quantum Chemistry: Classic Scientic Papers. World Scientic: Singapore, SG, 2000; 287.

[38] Barrell, H.; Sears, J.E. Philos. Trans. Roy. Soc. London Vol. 238, No. 786, 1, (1939).

[39] Ciddor, P.E. Appl. Opt. 35, 1567, (1996).

[40] Whiting, E.E. J. Quant. Spectrosc. Radiat. Transf. 8, 1379, (1968).